# Transient electroluminescence spikes in small molecular organic light-emitting diodes

Rui Liu, Zhengqing Gan, Ruth Shinar, and Joseph Shinar

Phys. Rev. B **83**, 245302 — Published 3 June 2011

DOI: 10.1103/PhysRevB.83.245302

# Comprehensive Investigation of Transient Electroluminescence Spikes in Small Molecular Organic Light-Emitting Diodes

Rui Liu,[1] Zhengqing Gan,[1] Ruth Shinar,[2*] and Joseph Shinar[1*]

[1]*Ames Laboratory – USDOE and Department of Physics and Astronomy, Iowa State University, Ames, IA 50011*

[2]*Microelectronics Research Center and Department of Electrical and Computer Engineering, Iowa State University, Ames, IA 50011*

## ABSTRACT

A comprehensive study of transient ns electroluminescence (EL) spikes that exceed the dc level and μs-long EL tails following a bias pulse in guest-host small molecular organic light-emitting diodes (SMOLEDs), including relatively efficient devices, which elucidates carrier and exciton dynamics in such devices, is presented. The transient EL is strongly dependent, among other parameters, on device materials and structure. At low temperatures, all measured devices, with the exception of Pt octaethylporphyrin (PtOEP)-doped tris(8-hydroxyquinoline) Al ($Alq_3$) SMOLEDs, exhibit the spikes at ~70-300 ns. At room temperature (RT), however, only those with a hole injection barrier, carrier-trapping guest-host emitting layer, and no strong electron-transporting and hole-blocking layer (such as 4,7-diphenyl-1,10-phenanthroline (BPhen)) exhibit strong spikes. These narrow and appear earlier under post-pulse reverse bias. To further elucidate the origin of the spikes, we monitored their dependence on the pulsed bias width and voltage, the doped layer thickness, and its location within the OLED structure. The characteristics of the μs-long tails were also evaluated through the effect of the post-pulse voltage. A model based on the recombination of

correlated charge pairs (CCPs) and on charge detrapping is presented; the model agrees well with the experimental data. The results suggest that reduced electric field-induced dissociative quenching of singlet excitons is responsible for the spikes' amplitude exceeding the on-pulse dc EL level. The long tails are attributed to recombination of charges detrapped from a distribution of shallow, mostly host, sites, reminiscent of the detrapping and recombination processes that yield the thermally stimulated luminescence of such materials. The comprehensive transient EL measurements in guest-host devices demonstrate the generality of the strong spike phenomenon in devices with charge trapping in the emitting guest molecules. Hence the transient EL can serve as an important tool to identify the dominant emitting mechanisms in the guest-host systems.

PACS Nos. 85.60.Jb, 78.60.Fi, 78.47.jd, 73.50.Gr

*Corresponding authors: rshinar@iastate.edu, jshinar@iastate.edu

## 1. INTRODUCTION

Thin film organic light emitting diodes (OLEDs) have advanced dramatically since they were first described.[1] They are comprised of one or multiple organic semiconducting layers, with a total thickness of ~100 nm, sandwiched between two electrodes. They exhibit great promise in various applications such as displays, solid-state lighting, and chemical and biological sensing.[2-7] However, despite growing interest and applications, fundamental processes that affect device performance, such as carrier transport and recombination, as well as electroluminescence (EL) quenching, in particular following a bias pulse, remain to be understood. In this study, we address these processes in small molecular OLEDs (SMOLEDs), which dominate OLED-based applications.

Most studies that address the above-mentioned processes focus on the behavior under dc voltage, with much less treatment of the transient behavior and its relation to device performance.[8-18] Among these studies, other than research concentrated on triplet-triplet annihilation (TTA) in long EL decay processes,[14,15] only a few transient EL studies on polymer LEDs (PLEDs)[8-10] and on 4,4'-bis(2,2'-diphenylvinyl)-1,1'-biphenyl (DPVBi)-based SMOLEDs[16,17] reported intriguing EL spikes following a bias pulse. Such spikes were also observed in (8-hydroxyquinoline) Al ($Alq_3$)-based[18] SMOLEDs but they were not analyzed. The observations reported in this paper point to these spikes as a general phenomenon in SMOLEDs, including relatively efficient devices, when charge trapping processes occur and, hence, result in a more comprehensive treatment of the transient EL behavior and its implications regarding the choice of OLED materials and device architecture. Additionally, as discussed later, the transient EL behavior may point to the light emission mechanism,

whether dominated by energy transfer from host to guest or by direct carrier trapping on the guest.

As is well known, the transport of carriers in amorphous organic solids is based on hopping between shallow localized states,[5-7] which is due to energetic or structural disorder and impurities. Traps within organic materials tend to retain charges for relatively long periods, as demonstrated by, e.g., thermally stimulated luminescence,[19] indicating that such long-lived trapped charges can survive after the external field is turned off. Unless they reach the appropriate electrode, such charges eventually form correlated charge pairs (CCPs) with an opposite mobile charge within the Onsager radius (19 nm at room temperature neglecting screening by other charges; <<19 nm if not).[17,20] The recombination of these carriers following a bias pulse will consequently affect the transient behavior of the OLEDs, both electrically and optically.

In this paper, a detailed investigation of transient EL spikes observed at 70 – 300 ns and tails extending to several μs following a bias pulse in efficient SMOLEDs is described. The effect of materials and other parameters/attributes of the various layers of the SMOLEDs are discussed, including the effect of temperature and post-pulse forward and reverse bias. The OLEDs studied comprised of all or part of the following layers: anode/hole injection layer (HIL)/hole transport layer (HTL)/guest-host emitting layer (EML)/hole blocking and electron transporting layer (HBL and ETL, respectively)/electron injection layer/metal cathode. Specific examples include EL spikes and tails in devices with coumarin6 (C6)-doped $Alq_3$) as the EML and copper phthalocyanine (CuPc) as the HIL. Since the highest occupied molecular orbital (HOMO) energy of C6 is $E_{HOMO} \approx$ -5.4 eV, it becomes a hole trapping center when

doped into $Alq_3$, where $E_{HOMO} \approx$ -5.9 eV. Hence, in this case (and other cases of a dopant that traps $h^+$ or $e^-$ due to its energy levels relative to the host), most of the CCPs will involve a relatively deeply trapped $h^+$ on the C6 and a relatively mobile $e^-$ hopping among the $Alq_3$ molecules around it. Thus the $e^-$ will eventually recombine with the $h^+$ to form an exciton on the C6.

The dependence of the spikes and tails on parameters such as the thickness of the doped layer and its distance from the HTL (*N,N*'-bis(naphthalen-1-yl)-*N,N*'- bis(phenyl)benzidine (α-NPB))/$Alq_3$ interface, the on-pulse voltage, the pulse duration, and the time the device was exposed to air are discussed. The strong effects of the HIL, whether absent, CuPc, or $MoO_3$, and of the ETL/HBL, are also discussed. Moreover, a model based on the observed phenomena is presented; the model is in good agreement with the experimental data. Based on the model and the experiments, the observed EL spikes are attributed to the recombination of CCPs, and the longer emission tails to recombination of initially unpaired, uncorrelated charges. Transient EL exhibiting spikes and tails observed in other doped devices are also presented. This comprehensive study highlights universal aspects of SMOLED performance. It points to the strong role of materials and device design as well as electric field-induced dissociative quenching of singlet excitons (SEs) (whose radiative decay yields the EL). The contribution from a "back-drift" of holes that have leaked through the recombination zone (RZ) toward the cathode and drift back toward the RZ in causing the EL spikes, as proposed for some PLEDs, is most likely marginal. Importantly, no spike is observed, even at low temperature, in a guest-host system where efficient energy transfer to a long-lived ($\tau_{rad} \sim$ 100 μs) phosphorescent guest, rather than charge trapping on it, dominates. This behavior can

possibly provide a novel way to distinguish between energy transfer and charge trapping processes in guest-host systems.

## 2. EXPERIMENTAL METHODS

21×21 OLED pixel arrays (pixel diameter ~1.5 mm) were fabricated combinatorially.[21] All depositions were performed in a conventional thermal vacuum evaporation chamber (base pressure ~$10^{-6}$ Torr; the organic layers' deposition rate was ~1 Å/s) installed inside a glove box with <20 ppm $O_2$. The bias pulses were generated by an Avtech Model AV-1011 power supply with a nominal rise and fall times of ~10 ns. The EL was monitored by a Hamamatsu R6060-02 photomultiplier tube (PMT) with a 50 Ω external load connected to a 350 MHz oscilloscope. For low temperature measurements, the OLED pixels' size was 2×2 $mm^2$. The devices were placed in a small chamber with a transparent window on one side. The EL was detected through that window using the PMT. Due to the geometry of the setup the PW in the low-temperature measurements was set to 1 ms to improve detection. As shown in the inset of Fig. 5, however, the difference in $A_{spike}$ using PWs of 100 μs and 1 ms is modest. Note that there were some variations in $A_{spike}$ from batch to batch, with the overall behavior reproducible.

## 3. RESULTS AND DISCUSSION

Following a bias pulse applied to an OLED several processes responsible for the post-pulse EL in fluorescent SMOLEDs occur.[22] These processes include:

(1) EL decay of pre-existing excitons, i.e., those formed during the pulse. This decay

process usually takes a few ns for SEs.[11,23]

(2) EL decay of SEs formed during the falling edge of the voltage pulse. Carriers are continuously injected into the device while the voltage is decaying, which in this work lasted for ≤ 50 ns.[24] The decaying external field also continues to drive the pre-existing electrons $e^-$ and holes $h^+$ from the bulk of the transporting layers into the RZ (which we approximate to coincide with the EML) to form excitons. The EL generated from these excitons, as well as from the pre-existing excitons of (1), results in an EL amplitude similar to that observed during the pulse.

(3) Recombination of initial CCPs (i.e., those present at $t$ ~50 ns after the end of the pulse). Even after the external field decays, charges within the RZ that are Coulombically bound, i.e., CCPs, recombine. The recombination of these charge pairs is believed to generate the EL spikes that are up to > 3 times larger than the on-pulse (dc) EL level. As discussed below, the intriguing strength of these EL spikes is suspected to be due to reduced electric-field-induced dissociative quenching of SEs as the applied field is turned off and the internal field due to the dissipating charge accumulation layers decays. An alternative mechanism, whereby increased CCP generation from holes that have leaked through the RZ, continued to drift toward the cathode, but now turn back toward the RZ in greater numbers due to the absence of an applied field,[22] is most likely marginal in generating the spikes.

(4) Recombination of newly formed CCPs. Detrapped charges originating mostly from host shallow states continue to pair with opposite charges, mostly on guest molecules, to form CCPs. Due to the relatively slow process of detrapping, the excitons generated from these CCPs yield the observed stretched exponential EL tails that extend over several

microseconds.

(5) Decay of SEs formed by TTA. The fusion of the triplets generates additional SEs, whose decay contributes to the transient EL. This process approximates an exponential decay in the long time range.[14] Compared to the EL decay caused by the trapped charges, TTA is not affected by the external electric field due to the charge neutrality of the triplets.

These processes for various materials, device structures, and conditions are discussed in detail in the following sections. We note that OLED displays can have a faster response time than standard LCD screens. While LCDs are capable of a ≤ 1 ms response time offering a frame rate ≥ 1 kHz, OLEDs are advantageous with potential response times < 10 μs (100 kHz refresh rates). However, the transient EL of OLEDs that might include a spike at ~100 ns and tails that extend to several μs (and even ms when triplet-triplet annihilation is non-negligible) present a limitation. This issue becomes increasingly acute as the display size increases. Moreover, the observed spikes and tails are already a limitation for the OLED-based luminescent biochemical sensing platform, which has been drawing considerable interest.[3,4]

### 3.1. Devices with CuPc as the HIL

#### *3.1.1. General Phenomena*

Fig. 1 shows a typical transient EL following a 100 μs, 6 V pulse, normalized to the EL amplitude during the pulse, in devices of the general structure ITO / CuPc (5 nm) / α-NPB (50 nm) / 1 wt.% C6:$Alq_3$ ($0 \le x \le 5$ nm) / $Alq_3$ (40-$x$ nm) / LiF (1 nm) / Al (~120 nm). These devices are termed A0 to A5, depending on the value of $x$. Strong EL spikes at ~100 ns and tails are observed in all C6-doped devices with CuPc as the HIL, but not in the undoped $Alq_3$ device A0. Similar spikes and tails were observed also in other device structures detailed

later.

As mentioned, C6, with $E_{HOMO} \approx$ -5.4 eV, is a hole trapping fluorescent dopant in $Alq_3$, where $E_{HOMO} \approx$ -5.9 eV. The emission is mainly through direct recombination of CCPs at the dopant molecules, resulting from carrier trapping.[25,26] As the carriers are driven toward the RZ during the bias pulse, $h^+$ are trapped on the energetically preferred sites of the C6 molecules. Although the CCPs will eventually recombine and form excitons, a considerable fraction of them and the resulting excitons could be dissociated by the electric field during the pulse, resulting in EL quenching. Research by other groups has shown that a significant amount of charges will be stored near the RZ under constant bias, causing a high internal electrical field.[27,28] It has also been shown that this field that induces SE dissociation can reduce the EL by > 60%.[29,30]

After the pulse is turned off there are many remaining CCPs in the RZ due to the holes trapped on the guest molecules. Since the electric field decreases, field-induced dissociative SE quenching is reduced as well, and the flow of $h^+$ that have leaked through the RZ toward the cathode and now turn back to the RZ increases.[8,9] The former process is believed to contribute to the EL spikes sufficiently to result in a spike amplitude that exceeds the on-pulse EL. Newly created CCPs, formed from unpaired, detrapped (mostly host) charges, are believed to contribute only to the EL tails, due to the slow process of detrapping and the larger distance from the RZ. The undoped $Alq_3$ device, on the other hand, has a much weaker post-pulse EL due to the lack of guest-host-related charge trapping sites and consequently CCPs. This observation therefore provides additional strong evidence for the charge trapping mechanism in the C6:$Alq_3$ guest-host system.

As seen in Fig. 1, the relative spike amplitude $A_{spike}$ (i.e., spike intensity normalized to the on-pulse level) increases when $x$ increases from 0 to 2 nm. This behavior is probably due to the increasing number of guest-induced traps. However, $A_{spike}$ decreases in device A5 in comparison to devices A1 and A2; repeated measurements reproduced this A5 weakened $A_{spike}$; in other devices, where the doped layer thickness was farther increased, the spike weakened further. Assuming that during the pulse the carrier density just outside the RZ is not drastically changed when the doped layer thickness increases, in A5 the internal electric field across the RZ is likely lower than in A2, which results in lower field-induced EL quenching during the pulse and hence a relatively lower $A_{spike}$.

To observe an EL spike, it is also important that excitons do not saturate the CCP sites. Fig. 2 shows $A_{spike}$ vs voltage in devices A1, A2, and A5. As clearly seen, $A_{spike}$ increases with the bias at low voltages, and decreases above ~6.5-7 V. Holes injected from the anode will be either trapped on guest molecules to later form CCPs, or will recombine with $e^-$ to form excitons in host or guest molecules. Due to the barrier for $h^+$ hopping from α-NPB to $Alq_3$, only a relatively small fraction of $h^+$ is supplied to the doped layer at low voltage, most of which will be rapidly trapped in the C6 guest molecules. Thus, the spike increases with bias as the trapped $h^+$ density in the guest molecules increases. When the bias is high (> ~6.5 V in this case), most of the guest traps are filled, and consequently the trapping rate decreases, while the guest+host exciton formation rates increase. Therefore, the relative amplitude of the spike decreases. This behavior and its analysis are similar (though not identical) to those of DPVBi-based OLEDs.[16,17]

*3.1.2. Effects of the Doped EML Position*

Fig. 3 confirms the crucial role of the C6:$Alq_3$ guest-host system in generating CCPs and hence the EL spikes. In addition to the normalized transient EL intensity of A0 and A1, it shows also the EL intensity in devices in which the 1 nm doped layer was fabricated at an increasing distance from the HTL. The general structure of these devices was ITO / CuPc (5 nm) / α-NPB (50 nm) / $Alq_3$ ($y$ nm) / 1 wt.% C6:$Alq_3$ (1 nm) / $Alq_3$ (39-$y$ nm) / LiF (1 nm) / Al (~120 nm) with $0 \leq y \leq 10$ nm; these devices are termed A1-1 to A1-10, based on the value of $y$. As seen in Fig. 3, the EL spike intensity decreased with increasing $y$. The $h^+$ energy barrier between α-NPB ($E_{HOMO} \approx$ -5.6 eV) and $Alq_3$ ($E_{HOMO} \approx$ -5.9 eV) obviously generates a $h^+$ accumulation layer at the α-NPB/$Alq_3$ interface, and therefore the carrier density in the guest-host layer decreases greatly as $y$ increases.[27] Hence, despite the unchanged doped-layer thickness, the carrier density in it, and consequently the CCP formation rate and its contribution to the spikes, decreases from A1-1 to A1-10. Since the contribution of $h^+$ that turn back toward the RZ after having drifted beyond it to the spikes should, if anything, increase with $y$, we conclude that this mechanism's contribution to the spikes is marginal.

*3.1.3. Ambient -Induced Degradation*

Fig. 4 shows the integrated transient EL of an unencapsulated A1 OLED as obtained from the integrated area $Q_{tot}$ and the normalized (relative to the 'on-pulse' level) integrated area $Q_N$ vs operation time. In spite of the decline of $Q_{tot}$ caused by degradation of the OLED, both the profile of the transient EL and $Q_N$ were barely changed. It indicates that the EL spikes and tails are an intrinsic property of the SMOLEDs that is related to the EML guest-host system,

device materials and structure, and carrier injection and transport energy barriers; it is not affected by early-stage ambient (likely humidity)-induced degradation mechanisms.

*3.1.4. Effects of Pulse Width*

Fig. 5 shows the dependence of the on-pulse EL and EL spike intensity on the applied bias pulse width (PW) for an A2 device. No spikes are observed when the PW is below 5 $\mu$s. The spike intensity increases sharply as the PW increases, but beyond 100 $\mu$s it saturates. When the PW increases, the bulk HTL and ETL carrier densities, in addition to the CCP density, increase, resulting in stronger electric field-induced EL quenching, which increases the difference between the EL spike intensity and the on-pulse EL. This behavior is in contrast to that of undoped and [2-methyl-6-[2-~(2,3,6,7-tetrahydro-1H, 5H-benzo [ij] quinolizin-9-yl)- ethenyl]-4H-pyran-4- ylidene] propane-dinitrile (DCM2)-doped DPVBi OLEDs,[16,17] where the normalized spike amplitude decreases beyond a PW of ~100 μs, clearly due to the subtle differences between the EL overshoot mechanisms in the $Alq_3$ and DPVBi-based devices. In the latter devices, there is a (modest) spike in the undoped OLEDs as well, and DCM2 traps both $h^+$ and $e^-$.[17] In the wide variety of the OLEDs described in this current study, when the PW is long enough for the device to reach a steady state, the relative spike intensity saturates due to the unchanged charge profile within the OLED.

**3.2. Model Analysis**

Based on the experiments described in the previous section and our interpretation of the origin of the EL spikes and tails, a model, accounting for the observations, was developed. As a brief summary, the major processes taken into account following the bias pulse in

fluorescent guest-host systems include

(*i*) EL decay of SEs formed during the pulse;

(*ii*) exciton formation from carriers injected into the RZ during the falling edge of the voltage pulse (i.e., during the 0 - 50 ns period following the pulse);

(*iii*) recombination of initial CCPs (those present at $t \sim 50$ ns);

(*iv*) recombination of newly formed CCPs generated from uncorrelated, detrapped carriers at $t > 50$ ns;

(*v*) decay of SEs formed from TTA.

In simulating the experimental results, the decay of the pre-existing SEs can be neglected, since their lifetime is < 10 ns.[11,23] Process (*v*) was not considered because its contribution is a significant component of the EL tail only at times beyond those monitored in this study.[14,15] Therefore, the EL spikes and tails were simulated as an exponential decay of SEs formed in processes (*ii*) - (*iv*).

The net SE formation rate $dN_{SE}(t)/dt$ is given by[22]

$$\frac{dN_{SE}(t)}{dt} = \left(\frac{dN_{exc}}{dt}\right)_J + N_{ccp0}R_{ccp}(t) + \int_0^t \frac{dN_e(t')}{dt'} R_{ccp}(t-t')dt' - \frac{N_{SE}(t)}{\tau_{SE}} \qquad (1).$$

The first term of Eq. (1) describes process (*ii*) in which the injected carriers' profile during the falling edge of the bias is proportional to the injection-limited current density $J$:[5,7]

$$\left(\frac{dN_{exc}}{dt}\right)_J \propto J \propto V(t)^2 \exp\left(-b/V(t)\right) \qquad (2).$$

The second term in Eq. (1) describes process (*iii*). In the initial CCPs (with initial density $N_{ccp0}$), subject to Coulomb attraction, the untrapped carrier performs a random walk toward the trapped carrier (usually localized on the guest). The recombination rate of these CCPs can

be written as:[20]

$$R_{ccp}(t) = \frac{\sqrt{4\pi}}{\sqrt{D_{ccp}}} \frac{r_c}{t^{3/2}} \int_0^\infty g(r_0) \exp\left(-\frac{r_0^2}{4D_{ccp}t}\right) \exp\left(-\frac{r_c}{r_0}\left(1 - \mathrm{erf}\left(\frac{r_0}{\sqrt{4D_{ccp}t}}\right)\right)\right) r_0^2 \, dr_0 \qquad (3).$$

where

$$g(r_0) = \frac{\exp\left(-\frac{(r_0 - \bar{r})^2}{\sigma^2}\right)}{4\pi^{3/2}\sigma\bar{r}^2} \qquad (4).$$

is a standard Gaussian distribution. In Eqs. (3) and (4) $D_{ccp}$ is the diffusivity of the mobile charge within the CCP, $r_c \sim 19$ nm is the room temperature Onsager radius,[17] $r_0$ is the $e^-$-$h^+$ separation within the CCP, $\bar{r}$ is the average of $r_0$, and $\sigma$ is the $r_0$ distribution width.

The third term in Eq. (1) is attributed to the recombination of detrapped charges. Due to the broad distribution of trap levels in organic materials,[31] the total density of trapped charges is approximated by a stretched exponential,[32,33] which is often used to describe charge transport and trapping governed by a distribution of relaxation times, in disordered systems

$$N_c(t) = N_c(0)\exp\left(-(t/\tau_{ucc})^{\beta}\right) \qquad (5)$$

$\beta$ is the stretching factor that quantifies the distribution width of the trapping energies, and $\tau_{ucc}$ is the characteristic time the carrier remains uncorrelated.

The fourth term in Eq. (1) presents the loss of SEs due to the radiative and various nonradiative decay channels.

By solving Eq. (1), the time-dependent $N_{SE}(t)$ can be expressed as:[22]

$$N_{SE}(t) = N_e \exp\left(-\frac{t}{\tau_{SE}}\right) + N_{ccp0} \exp\left(-\frac{t}{\tau_{SE}}\right) \int_0^t R_{ccp}(t') \exp\left(\frac{t'}{\tau_{SE}}\right) dt' + \exp\left(-\frac{t}{\tau_{SE}}\right) \int_0^t \exp\left(\frac{t'}{\tau_{SE}}\right) \left[\int_0^{t'} \frac{dN_c(s)}{ds} R_{ccp}(t' - s)\, ds\right] dt' \qquad (6)$$

where $N_e = \int_0^t \left(\frac{dN_{EXC}}{dt'}\right)_I \exp\left(\frac{t'}{\tau_{SE}}\right) dt' + Constant$. The first, second, and third terms of Eq. 6 are due to excitons generated from process (*ii*), (*iii*) and (*iv*), respectively. In the second and third terms the $t = 0$ lower limit of the integrals corresponds to $t = 50$ ns in the experiments. Due to the fast decay of the SEs and the recombination of CCPs compared to the detrapping rate, the third term of Eq. (6) can be approximated by the stretched exponential (Eq. (5)).

Fig. 6 shows the log-log plot of the normalized transient EL profile for device A2 after a 100 $\mu$s bias pulse with on-pulse amplitudes of 7, 9, and 11 V. The solid lines show the best fit using Eq. (6). The separate contributions of processes (*ii*) + (*iii*) and process (*iv*) (governed by the stretched exponential dynamics) are plotted as the dashed and dotted lines, respectively. As clearly seen, the model is in good agreement with the observed behavior *over the whole observed transient EL period*. In particular, the agreement is better than that obtained using a CCP + Langevin recombination model described previously.[17]

Fitting Eq. (6) to the observed behavior yields the SE decay time $\tau_{SE} = 8.7$ ns, which is consistent with the C6 radiative lifetime $\tau_{rad} < 10$ ns.[12,23] It also yields a practically unchanged $D_{ccp} \sim 5.6\times10^{-7}$ cm$^2$/s. This implies a mobility of $\sim 2\times10^{-5}$ cm$^2$/V·s, which is reasonable given the fact that the holes are trapped and the relative movement within the CCPs is dominated by the mobile electrons hopping among $Alq_3$ molecules.[34]

The inset of Fig. 6 shows the dependence of $\bar{r}$ and $\tau_{ccp}$ on the bias. The fit yields $\bar{r}$ = 4.9, 3.9, and 3.7 nm and $\tau_{ccp}$ = 115, 68, 63 ns at 7, 9, and 11 V, respectively, where $\tau_{ccp} = \bar{r}^2/(4D_{ccp})$. The decrease in $\bar{r}$ is obviously due to the increased carrier density and consequently decreased $\tau_{ccp}$, but both level off above ~9 V where $\bar{r} \approx 3.7$ nm.

At $t < 200$ ns, the first and second terms of Eq. (6) dominate. At longer times the free

carrier density decreases, and the detrapping process increasingly dominates. The dotted lines in Fig. 6 represent the contribution of the detrapping process that, as mentioned, is governed by the stretched exponential behavior (Eq. (5)). The fitting of the long tails and Eq. (5) yield $\bar{\tau}_{ucc}$ = 0.74, 0.86, and 1.05 μs for 7, 9, and 11 V, respectively, where $\bar{\tau}_{ucc} = (\tau_{ucc}/\beta)\Gamma(1/\beta)$, and $\Gamma$ is the gamma function.[35] The respective values of $\beta$ are 0.38, 0.48, and 0.59. The increase in $\beta$ with $V$ is expected, as the additional charges likely occupy a narrower range of energies in shallower tail states. The increase of $\bar{\tau}_{ucc}$ with $V$ may be due to the increasing imbalance between the saturated $h^+$ trapping sites in the C6 guests and the increased density of $e^-$ in the shallow host $Alq_3$ states.

Fig. 7 shows the fit of the model to the transient EL in OLEDs with different doped layer thickness following a 10 V bias pulse. Note that the relative intensity of the long tail at a given $V$ increases with increasing thickness of the doped layer $x$, indicating that most of the tail emission is due to C6. The fit of Eq. (5) to the long tails yields $\bar{\tau}_{ucc}$ = 0.57, 0.92, and 1.01 μs for A0, A2, and A5, respectively, at $V$ = 10 V. This increase in $\tau_{ucc}$ with doped layer thickness is probably due to the longer time needed for the detrapped carriers to find the opposite charges and form an exciton.

### 3.3. Effect of the HIL and ETL/HBL in C6-doped $Alq_3$-based devices

The observation of EL spike with an amplitude greater than the on-pulse level is intriguing and elucidating their nature is therefore challenging. In order to further evaluate the above-mentioned model and elucidate the origin of the spikes, additional C6-doped $Alq_3$-based devices with different materials/structures were fabricated; their transient EL behavior is shown in Fig. 8. In particular, the influence of the HIL and ETL/HBL on the EL

spikes was investigated. The structures are (a) a device without any HIL; (b) a control device A1 with CuPc as the HIL; (c) a device with CuPc as the HIL and an added ETL/HBL of 4,7-diphenyl-1,10- phenanthroline (BPhen), where the total thickness of the device is kept constant; (d) a device with $MoO_3$ as the HIL, with no added BPhen.

As seen in Fig. 8, the normalized $A_{spike}$ decreased from structure (a) to (b) to (c). No EL spikes were observed in device (d) or in a device with both $MoO_3$ and BPhen (not shown). BPhen is a well known ETL/HBL material,[36] while $MoO_3$ greatly improves hole injection.[37,38] In comparing the devices shown in Fig. 8(a) (no HIL), (b) (CuPc as HIL) and (d) ($MoO_3$ as HIL), the EL spike decreases and even disappears as the $h^+$ injecting energy barrier is lowered. In comparing devices (b) (no ETL/HBL) and (c) (BPhen added) of Fig. 8, the EL spikes are reduced as the BPhen is added. Based on these observations, we conclude that in addition to a sufficient trapped carrier density in the RZ (as discussed in section 2.1) a sufficiently high $h^+$ injection barrier and the absence of a ETL/HBL are also crucial for creating strong transient EL spikes.

The foregoing results suggest that the mechanism that is likely responsible for EL spikes whose amplitude exceeds the on-pulse intensity is reduced electric field-induced dissociative SE quenching.[29] The high barrier for $h^+$ injection in devices with CuPc or no HIL results in a large accumulation of $h^+$ at the ITO/α-NPB or ITO/CuPc interface, respectively, when biased. This high $h^+$ density increases the internal field, which dissociatively quenches SEs during the bias pulse. When the bias is turned off, this $h^+$ accumulation layer dissipates as the $h^+$ diffuse, mostly back to the anode, resulting in much less field-induced SE dissociative quenching. When $MoO_3$ is used as the HIL, $h^+$ injection is greatly improved. This

improvement increases the carrier density within the bulk of the organic materials and forces the major accumulation of carriers to occur at the α-NPB/$Alq_3$ interface. In this way the internal electric field is higher and slower to decay, and consequently continues to suppress the EL after the bias is turned off, and therefore no spike is observed.

The observation that BPhen reduces the spike is probably due to the enhanced $e^-$ mobility in that material (~50 times higher than in $Alq_3$[36]), which probably reduces $h^+$ buildup at the α-NPB/$Alq_3$ interface and in the RZ.

An alternative mechanism, namely increased fraction of $h^+$ that have leaked through the RZ, drift toward the cathode, and then "turn back" toward the RZ, is ruled out as a major contributor to the spikes. This is due to at least two observations: (a) The RT spike is absent from the undoped devices; a significant contribution from $h^+$ beyond the RZ that turn back toward it would mandate a significant spike in the undoped devices as well. (b) As mentioned in Sec. 2.1, the contribution of $h^+$ that turn back toward the RZ after having drifted beyond it to the spikes should, if anything, increase with $y$, in sharp contrast to the observed strong decrease in $A_{spike}$ with increasing $y$ (Fig. 3).

### 3.4. Effect of Post-Pulse Reverse Bias

Fig. 9 shows the transient EL behavior of device A1 under post-pulse reverse and forward bias. When a forward bias is applied, the post-pulse internal electric field is slower to decay as more charges continue to be injected into the RZ, which results in suppression of the EL spike and a much higher emission tail. Under reverse bias, the decay of the internal electric field becomes faster and the spike appears earlier with a weakened tail. This behavior

strongly supports the conclusion that the transient EL tail results from trapped charges rather than TTA because, as mentioned, neutral triplets should not be affected by the external field.

### 3.5. Effect of Temperature

Fig. 10 shows the dependence of the EL spikes on the temperature in the 40 to 300 K range. A 1 ms pulse was used to achieve a sufficiently high EL intensity in the low-temperature measurements. As shown in the inset of Fig.5, the pulse width difference (between 100 μs and 1 ms) does not affect the transient behavior. Both A0 and A1 exhibit strong EL spikes at low temperatures, while only A1 shows an EL spike at room temperature.[39] At low temperatures, carriers are more prone to trapping in shallow traps as well. Their reduced mobility then suggests a much higher charge density within the RZ after the end of the pulse. This should lead to a higher concentration of CCPs and a strong internal electric field during the pulse that quenches the EL, yielding a larger difference between the transient and on-pulse EL; Fig. 10 supports this interpretation.

### 3.6. Transient EL in Other SMOLEDs

The transient EL behavior was studied in other efficient SMOLEDs of different materials. These include rubrene-doped $Alq_3$, *fac* tris(2-phenylpyridine) Ir ($Ir(ppy)_3$)-doped spiro-4,4'-Bis(9-carbazolyl) biphenyl (spiro-CBP), and Pt(II) octaethylporphine (PtOEP)-doped $Alq_3$ SMOLEDs. The observations confirm the occurrence of EL spikes and tails in various guest-host SMOLEDs where charge trapping is dominant and prove that the phenomenon appears to be universal even in some phosphorescent OLEDs where triplet excitons are the emitting species. Fig. 11 exhibits the transient EL behavior of devices with a rubrene-doped $Alq_3$, $Ir(ppy)_3$-doped spiro-CBP, and PtOEP-doped $Alq_3$ EML. As seen in the

figure, EL spikes are observed in the first two, but not in the PtOEP-doped device, even at 20 K. This situation can be attributed to two phenomena: the emission of PtOEP-doped $Alq_3$ guest-host system is dominated by strong energy transfer,[40] and the long radiative decay time of this phosphorescent molecule is $\tau_{rad} \sim 100$ μs. In contrast, the emission mechanisms of the $Ir(ppy)_3$- and rubrene-doped devices are both known to originate from charge trapping.[40,41] Note that the spikes in the rubrene-doped devices are stronger than those in the C6- and $Ir(ppy)_3$-doped SMOLEDs. This behavior supports the CCP model since it is well known that rubrene is a stronger $h^+$ trap in $Alq_3$. Hence, the EL spikes appear to be a reliable and easily measurable phenomenon to identify the main emitting mechanism in guest-host OLEDs.

## 4. CONCLUSIONS

In conclusion, following a bias pulse, ITO/CuPc/α-NPB/C6-doped $Alq_3$/$Alq_3$/LiF/Al devices and other charge trapping guest-host SMOLEDs exhibit EL spikes at 70 – 300 ns and μs long EL tails, whose amplitude varies with the pulse voltage. The spikes are not affected by early-stage device degradation, but are strongly influenced by the pulse duration and the distance of the doped layer from the HTL. They narrow and shift to shorter times under a reverse bias applied after the pulse. At low temperature they are much stronger, appear after a slightly longer time, *and are apparently universal in all charge-trapping SMOLEDs*, with the exception of devices in which there is efficient energy transfer to a long-lived phosphorescent guest emitter. Good agreement is found between the experimental data and a model based on recombination of CCPs and charges that are initially unpaired. The generation of spikes exceeding the on-pulse EL level is attributed to the combination of CCP formation and reduced electric field-induced SE dissociation after the pulse. The spikes are significantly

weaker in devices where a BPhen ETL/HBL layer is added, likely due to enhanced $e^-$ transport, and absent in devices where $MoO_3$ replaces CuPc.

The comparison of the transient EL behavior of various SMOLEDs suggests that the EL spikes are an additional reliable tool to identify the main emitting mechanism in guest-host OLEDs.

**ACKNOWLEDGEMENTS**

Ames Laboratory is operated by Iowa State University for the US Department of Energy (USDOE) under Contract No. DE-AC 02-07CH11358. This work was supported by the Director for Energy Research, Office of Basic Energy Sciences, USDOE.

**FIGURE CAPTIONS**

**Fig. 1.** The transient EL following a 100 μs, 6.0 V pulse of devices of the structure ITO/5 nm CuPC/50 nm α-NPB/*x* nm 1wt% C6:$Alq_3$/(40-*x*) nm $Alq_3$/1 nm LiF/~120 nm Al, termed, device A*x* (i.e., A0, A1, A2, A5). Inset: Expanded view of the transient EL up to 200 ns following the bias pulse.

**Fig.2.** The voltage dependence of the peak intensity of the spike in A1 (open circles), A2 (solid squares), and A5 (solid triangles). The lines are a guide to the eye.

**Fig.3.** The EL, following a 100 μs, 6.0 V pulse, of undoped $Alq_3$ device A0 (solid squares), C6-doped device A1 with the doped layer at the α-NPB/$Alq_3$ interface (open circles), and A1-based devices, A1-*y*, with the doped layer at distance *y* from the HTL, i.e., ITO/5 nm CuPC/50 nm α-NPB/*y* nm $Alq_3$/1 nm 1wt% C6:$Alq_3$/(39-*y*) nm $Alq_3$/1 nm LiF/~120 nm. The A1-*y* devices, according to the value of *y*, are A1-1 (solid triangles), A1-2 (open inverted triangles), A1-5 (stars), and A1-10 (open diamonds).

**Fig. 4**. The integrated area of the transient EL of unencapsulated device A1 operated constantly at 9V, $Q_{tot}$, (solid squares) and the normalized value, $Q_N$, (open circles) vs. the OLED's operation time.

**Fig. 5.** The pulse width dependence of the on-pulse EL (solid squares) and EL spike (open circles) intensities of device A2. Inset: Dependence of the EL spike intensity normalized to the on-pulse intensity of A2 on the bias pulse width.

**Fig. 6.** Log-log plot of the transient EL of device A2 following 7 V (circles), 9 V (squares), and 11 V (triangles) pulses. The solid lines are the best fits using Eq. (6). The dashed and dotted lines are the contributions of the excitons and CCPs present at $t$ = 50 ns, and detrapped carriers (governed by a stretched exponential), respectively. Inset: the voltage dependence of $\tau_{ccp}$ and $\bar{r}$; the lines are guides to the eye.

**Fig. 7.** The transient EL decay of A0 (circles), A2 (squares), and A5 (triangles) following a 10 V bias pulse with 100 $\mu$s duration. The solid lines are the least square fits of Eq. (6); the dashed lines are the fits of the stretched exponential (Eq. 5). The inset is the semi-log plot expansion showing the spikes.

**Fig. 8.** The transient EL following a 100 μs bias pulse for four devices with different structures, normalized to the on-pulse level. (a) ITO/50 nm α-NPB/2 nm 1wt% C6 doped-$Alq_3$/38 nm $Alq_3$/1 nm LiF/~120 nm Al, i.e, no HIL; (b) ITO/5 nm CuPc/50 nm α-NPB/2 nm 1wt% C6 doped-$Alq_3$/38 nm $Alq_3$/1 nm LiF/~120 nm Al, i.e., CuPc as the HIL; (c) ITO/5 nm CuPc/50 nm α-NPB/2 nm 1wt% C6 doped-$Alq_3$/38 nm $Alq_3$/30 nm BPhen/1nm LiF/~120nm Al, i.e., a BPhen HBL was added to structure (b); (d) ITO/5 nm $MoO_3$/50 nm α-NPB/2 nm 1wt% C6 doped-$Alq_3$/38 nm $Alq_3$/1 nm LiF/~120 nm Al, i.e., structure (b)

where $MoO_3$ replaced CuPc as the HIL. The lines are the simulations based on Eq. 6.

**Fig. 9.** The normalized transient EL data (symbols) and simulations (lines) with 100 μs, 9 V bias pulses at post-pulse voltages of 4 V (a), 0 V (b), -4 V (c), and -8V (d).

**Fig. 10.** The experimental, normalized EL (symbols) and simulated EL (lines) of devices A0 (a) and A1 (b) at temperatures $40 \leq T \leq 300$ K. The applied bias PW was 1 ms to achieve a high enough EL intensity with the low temperature measurements set-up.

**Fig. 11.** The transient EL of different guest-host SMOLEDs, all with structure ITO / 5 nm CuPc / 50 nm α-NPB / guest-host EML / 40 nm $Alq_3$ / 1 nm LiF / ~120 nm Al. EML is (a) 1 nm 1 wt.% rubrene in $Alq_3$, at RT, 8 V, 100 μs pulse, (b) 1 nm 6 wt% $Ir(ppy)_3$ doped-spiro CBP, at RT, 8 V, 100 μs pulse, (c) & (d) 1 nm and 2 nm 6 wt.% PtOEP doped-$Alq_3$ with 600 nm long-pass filter at RT, 7 V, 100 μs pulse and 20 K, 24 V, 1 ms pulse, respectively.

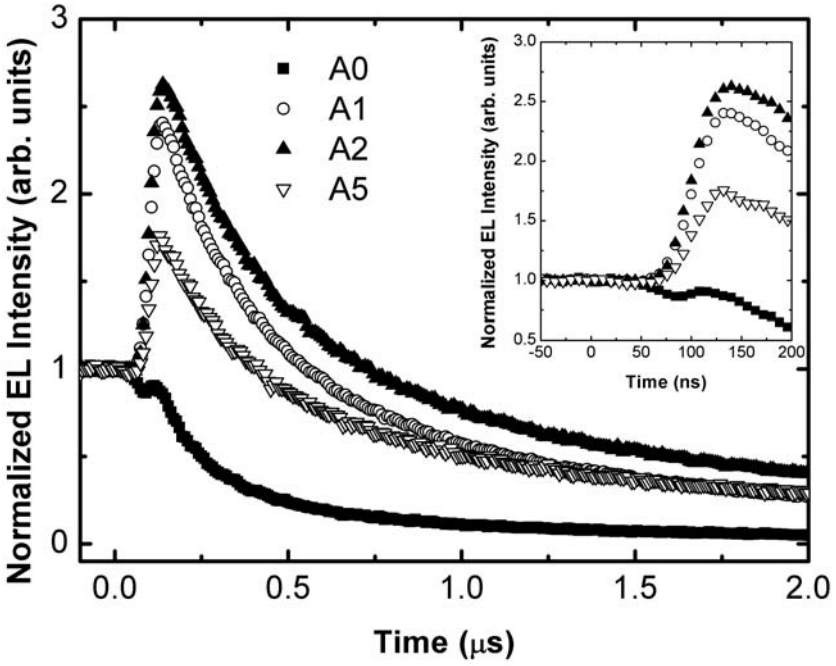


**Fig. 1.** The transient EL following a 100 μs, 6.0 V pulse of devices of the structure ITO/5 nm CuPC/50 nm α-NPB/*x* nm 1wt% C6:$Alq_3$/(40-*x*) nm $Alq_3$/1 nm LiF/~120 nm Al, termed, device A*x* (i.e., A0, A1, A2, A5). Inset: Expanded view of the transient EL up to 200 ns following the bias pulse.

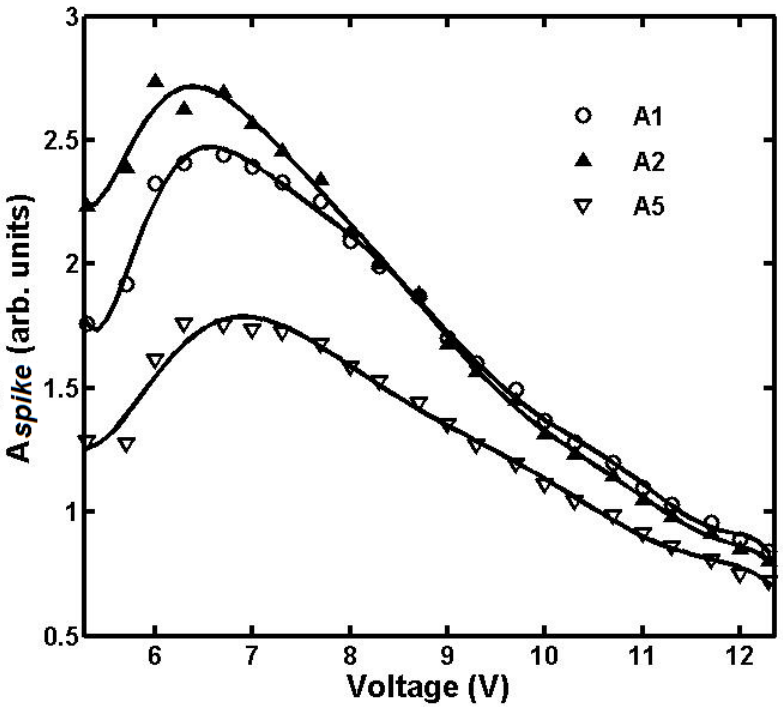


**Fig.2.** The voltage dependence of the peak intensity of the spike in A1 (open circles), A2 (solid squares), and A5 (solid triangles). The lines are a guide to the eye.

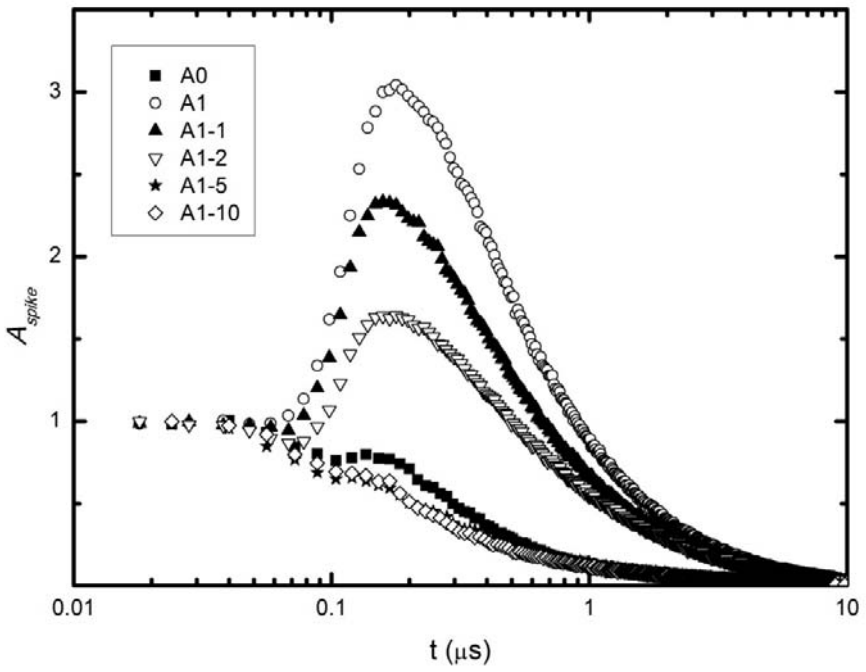


**Fig.3.** The EL, following a 100 μs, 6.0 V pulse, of undoped $Alq_3$ device A0 (solid squares), C6-doped device A1 with the doped layer at the α-NPB/$Alq_3$ interface (open circles), and A1-based devices, A1-*y*, with the doped layer at distance *y* from the HTL, i.e., ITO/5 nm CuPC/50 nm α-NPB/*y* nm $Alq_3$/1 nm 1wt% C6:$Alq_3$/(40-*y*) nm $Alq_3$/1 nm LiF/~120 nm. The A1-*y* devices, according to the value of *y*, are A1-1 (solid triangles), A1-2 (open inverted triangles), A1-5 (stars), and A1-10 (open diamonds).

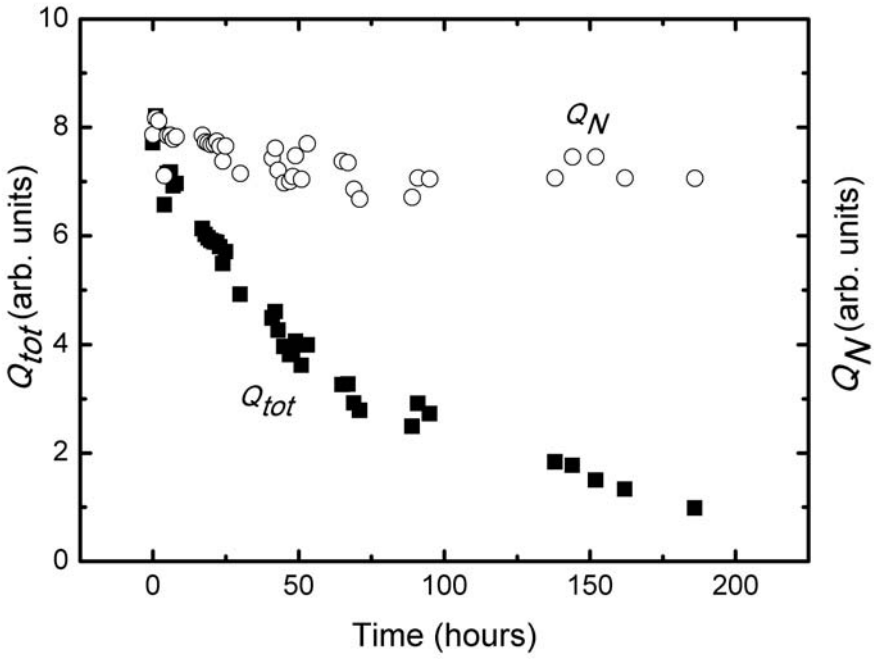


**Fig. 4**. The integrated area of the transient EL of unencapsulated device A1 operated constantly at 9V, $Q_{tot}$, (solid squares) and the normalized value, $Q_N$, (open circles) vs. the OLED's operation time.

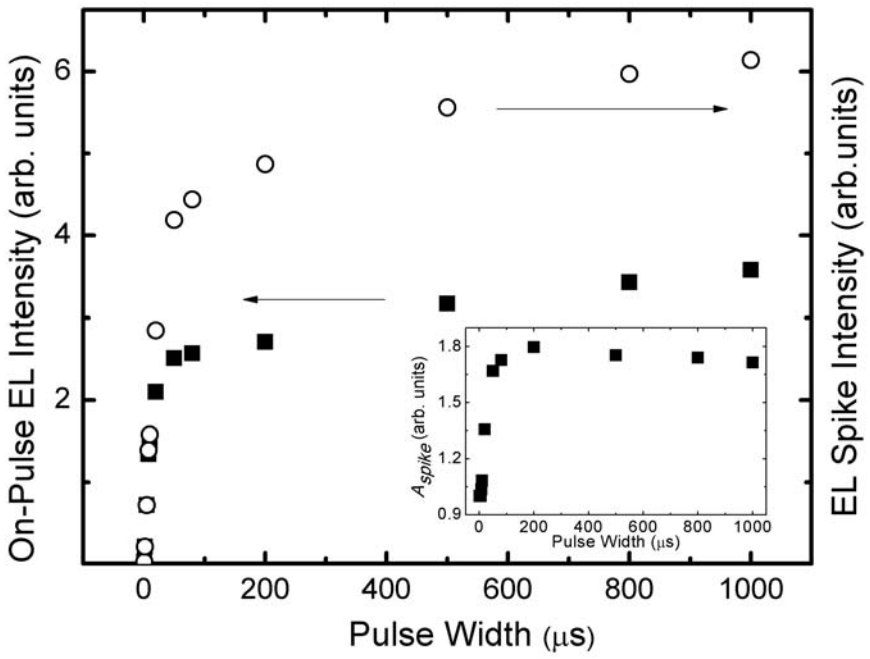


**Fig. 5.** The pulse width dependence of the on-pulse EL (solid squares) and EL spike (open circles) intensities of device A2. Inset: Dependence of the EL spike intensity normalized to the on-pulse intensity of A2 on the bias pulse width.

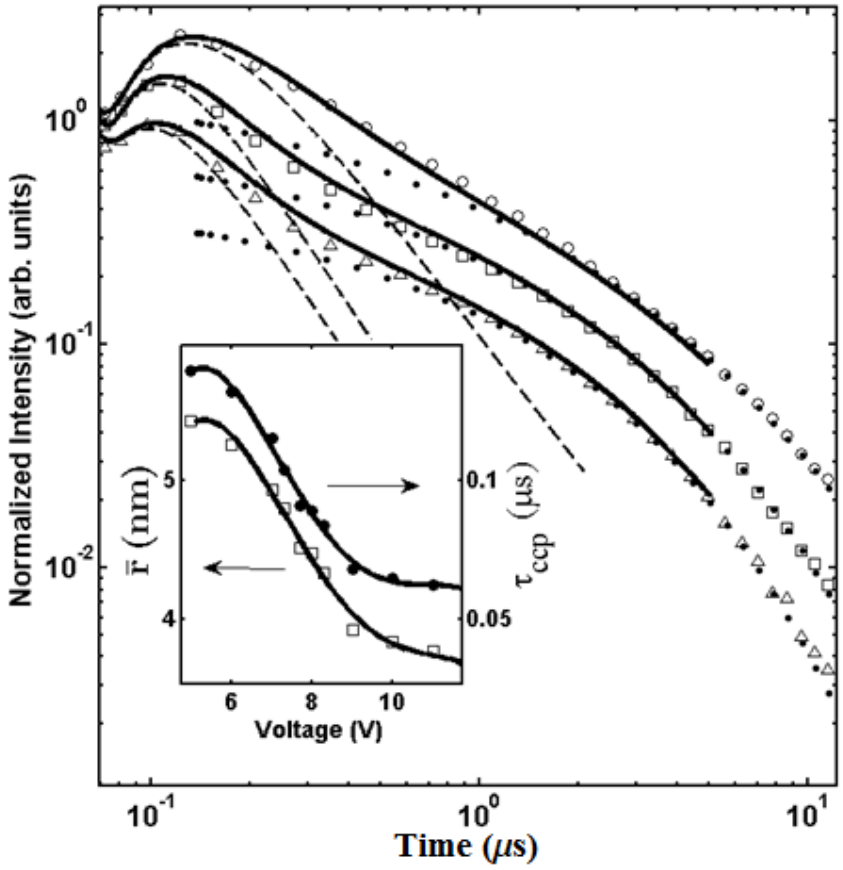


**Fig. 6.** Log-log plot of the transient EL of device A2 following 7 V (circles), 9 V (squares), and 11 V (triangles) pulses. The solid lines are the best fits using Eq. (6). The dashed and dotted lines are the contributions of the excitons and CCPs present at $t$ = 50 ns, and detrapped carriers (governed by a stretched exponential), respectively. Inset: the voltage dependence of $\tau_{ccp}$ and $\bar{r}$; the lines are guides to the eye.

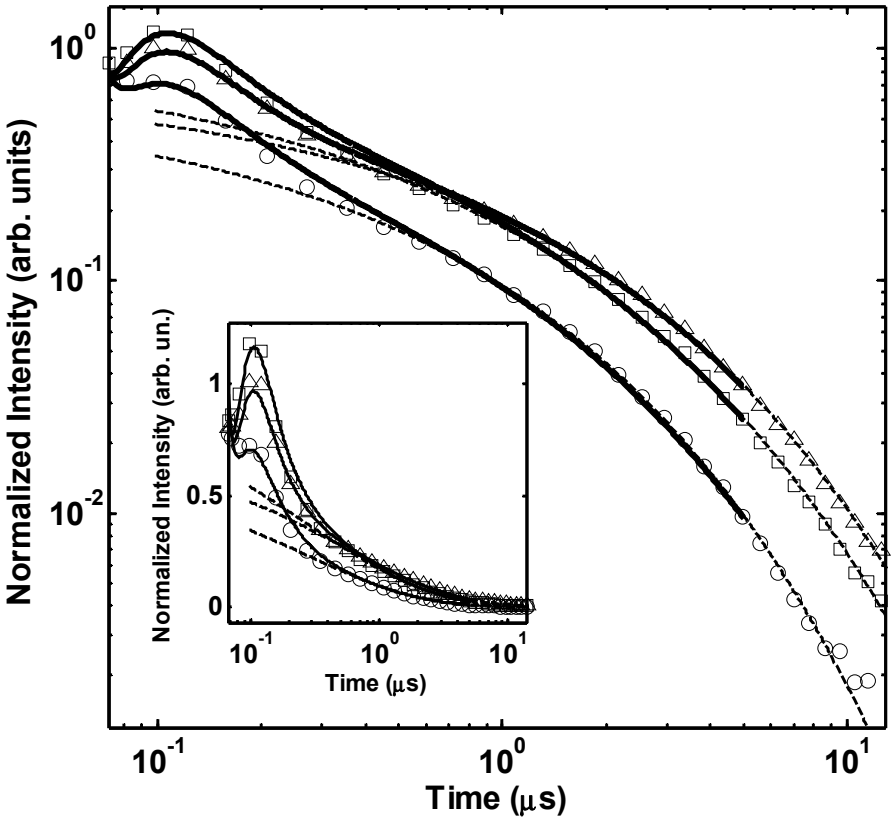


**Fig. 7.** The transient EL decay of A0 (circles), A2 (squares), and A5 (triangles) following a 10 V bias pulse with 100 $\mu$s duration. The solid lines are the least square fits of Eq. (6); the dashed lines are the fits of the stretched exponential (Eq. 5). The inset is the semi-log plot expansion showing the spikes.

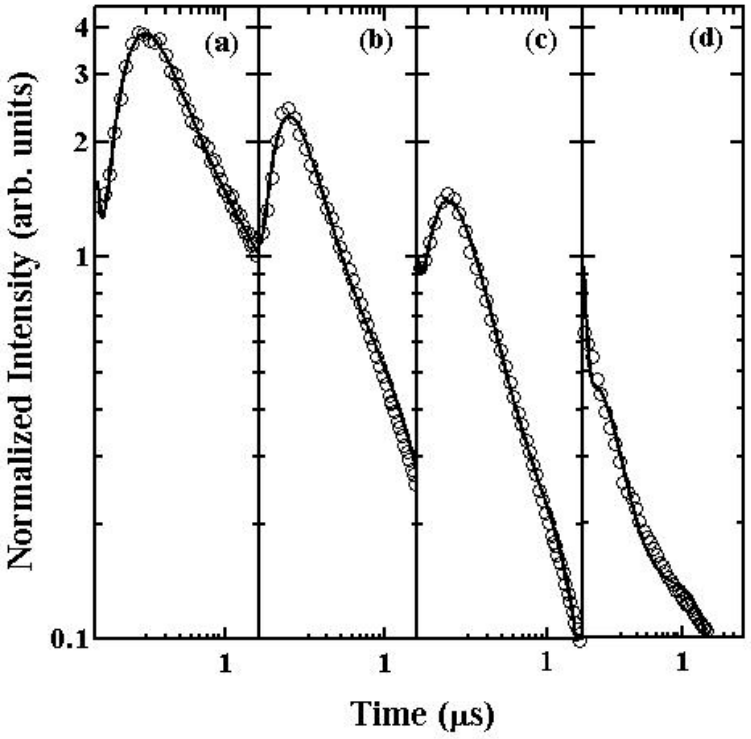


**Fig. 8.** The transient EL following a 100 μs bias pulse for four devices with different structures, normalized to the on-pulse level. (a) ITO/50 nm α-NPB/2 nm 1wt% C6 doped-$Alq_3$/38 nm $Alq_3$/1 nm LiF/~120 nm Al, i.e, no HIL; (b) ITO/5 nm CuPc/50 nm α-NPB/2 nm 1wt% C6 doped-$Alq_3$/38 nm $Alq_3$/1 nm LiF/~120 nm Al, i.e., CuPc as the HIL; (c) ITO/5 nm CuPc/50 nm α-NPB/2 nm 1wt% C6 doped-$Alq_3$/38 nm $Alq_3$/30 nm BPhen/1nm LiF/~120nm Al, i.e., a BPhen HBL was added to structure (b); (d) ITO/5 nm $MoO_3$/50 nm α-NPB/2 nm 1wt% C6 doped-$Alq_3$/38 nm $Alq_3$/1 nm LiF/~120 nm Al, i.e., structure (b) where $MoO_3$ replaced CuPc as the HIL. The lines are the simulations based on Eq. 6.

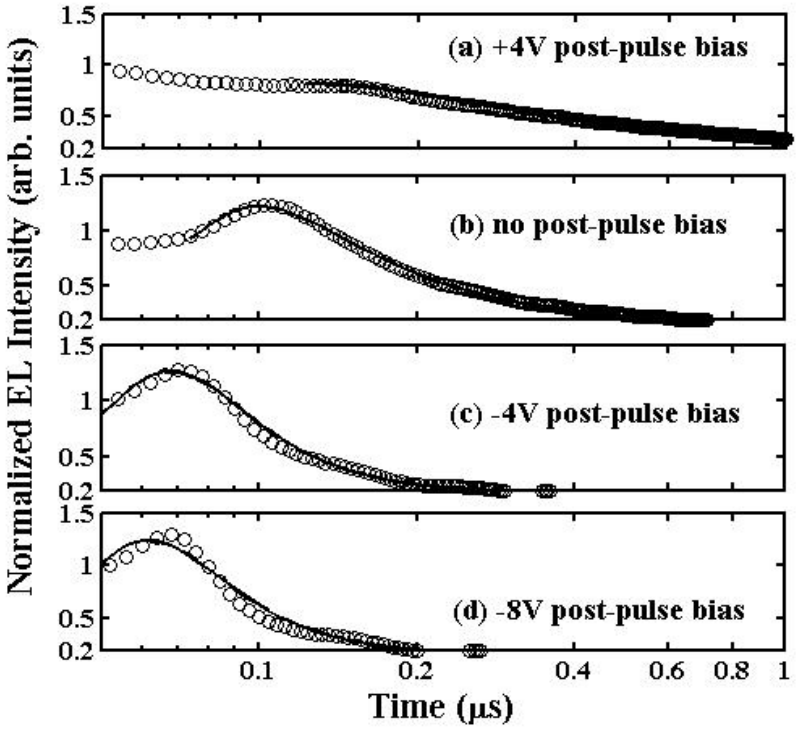


**Fig. 9.** The normalized transient EL data (symbols) and simulations (lines) with 100 μs, 9 V bias pulses at post-pulse voltages of 4 V (a), 0 V (b), -4 V (c), and -8V (d).

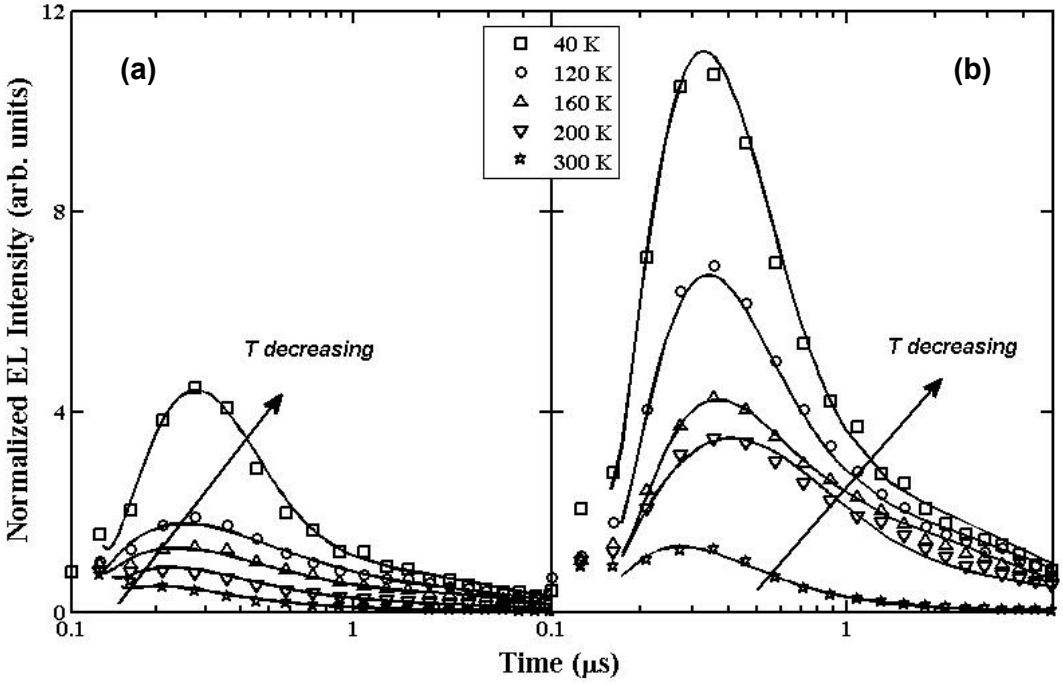


**Fig. 10.** The experimental, normalized EL (symbols) and simulated EL (lines) of devices A0 (a) and A1 (b) at temperatures $40 \leq T \leq 300$ K. The applied bias PW was 1 ms to achieve a high enough EL intensity with the low temperature measurements set-up.

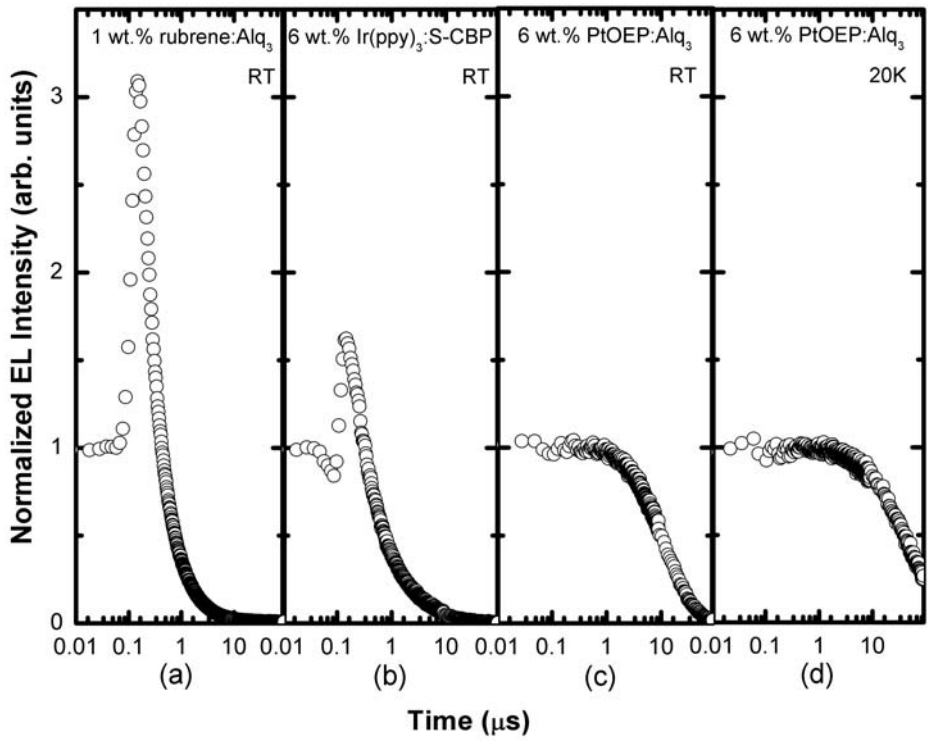


**Fig. 11.** The transient EL of different guest-host SMOLEDs, all with structure ITO / 5 nm CuPc / 50 nm α-NPB / guest-host EML / 40 nm $Alq_3$ / 1 nm LiF / ~120 nm Al. EML is (a) 1 nm 1 wt.% rubrene in $Alq_3$, at RT, 8 V, 100 μs pulse, (b) 1 nm 6 wt% $Ir(ppy)_3$ doped-spiro CBP, at RT, 8 V, 100 μs pulse, (c) & (d) 1 nm and 2 nm 6 wt.% PtOEP doped-$Alq_3$ with 600 nm long-pass filter at RT, 7 V, 100 μs pulse and 20 K, 24 V, 1 ms pulse, respectively.

**REFERENCES**


1. C. W. Tang and S. A. Vanslyke, Appl. Phys. Lett. **51**, 913 (1987)
2. R. F. Service, Science **310**, 1762 (2005)
3. J. Shinar and R. Shinar, J. Phys. D **41**, 133001 (2008).
4. *Organic Electronics in Sensors and Biotechnology* (Eds: R. Shinar and J. Shinar, McGraw Hill, NY, 2009).
5. J. Shinar and V. Savvate'ev, in *Organic Light Emitting Devices: A Survey* (Ed: J. Shinar, Springer Verlag, NY, 2004), Ch. 1.
6. *Organic Electroluminescence* (Ed: Z. Kafafi, Taylor & Francis, CRC Press, Boca Raton, FL 2005).
7. J. Kalinowski, *Organic Light-Emitting Diodes: Principles, Characteristics, and Processes* (Marcel Dekker, NY, 2005).
8. Y. H. Tak, J. Pommerehne, H. Vestweber, R. Sander, and H. Bässler, Appl. Phys. Lett. **69**, 1291 (1996).
9. V. R. Nikitenko, V. I. Arkhipov, Y.-H. Tak, J. Pommerehne, H. Bässler, and H.-H. Hörhold, J. Appl. Phys. **81**, 7514 (1997).
10. J. M. Lupton, V. R. Nikitenko, I. D. W. Samuel, and H. Bässler, J. Appl. Phys. **89**, 311(2001).
11. D. J. Pinner, R. H. Friend, and N. Tessler, J. Appl. Phys. **86**, 5116 (1999).
12. J. Kalinowski, N. Camaioni, P. Di Marco, V. Fattori, and A. Martelli, Appl. Phys. Lett. **72**, 513 (1998).
13. M. A. Baldo, C. Adachi, and S. R. Forrest, Phys. Rev. B **62**, 10967 (2000)

14. Z. D. Popovic and H. Aziz, J. Appl. Phys. **98**, 013510 (2005).

15. D. Y. Kondakov, J. Appl. Phys. **102**, 114504 (2007).

16. V. Savvateev, J. H. Friedl, L. Zou, J. Shinar, K. Christensen, W. Oldham, L. J. Rothberg, Z. Chen-Esterlit, and R. Kopelman, Appl. Phys. Lett. **76**, 1501(2000).

17. K. O. Cheon and J. Shinar, Phys. Rev. B **69**, 201306 (2004).

18. S. C. Tse, H. H. Fong, and S. K. So, J. Appl. Phys. **94**, 2033 (2003).

19. A. Kadashchuk, V. I. Arkhipov, C.-H. Kim, J. Shinar, D.-W. Lee, Y.-R. Hong, J.-I. Jin, P. Heremans, and H. Bässler, Phys. Rev. B **76**, 235205 (2007).

20. A. Mozumder, J. Chem. Phys. **48**, 1659 (1968).

21. L. Zou, V. Savvate'ev, J. Booher, C.-H. Kim, and J. Shinar, Appl. Phys. Lett. **79**, 2282 (2001).

22. Z. Gan, R. Liu, R. Shinar, and J. Shinar, Appl. Phys. Lett. **97**, 113301 (2010).

23. T. Nakazawa, M. Asano, S. Fujita, and S. Fujita, Jpn. J. Appl. Phys., Part 2 **38**, L206 (1999).

24. (i) The pulsed bias was provided by an Avtech Model AV-1011 Pulse Generator, with bias rise and fall times of ~10 ns. (ii) The field-dependent electron mobility in $Alq_3$ and hole mobility in α-NPB are ~$10^{-4}$ $cm^2/Vs$, so if the potential drop across each of these layers is ~4 V, then the time required to drift through the ~45 nm-thick HTL & ETL is ~$(45\times10^{-7}cm)^2/(4V\times10^{-4}\ cm^2/Vs)$ = 50 ns.

25. J. Kido and Y. Iizumi, Appl. Phys. Lett. **73**, 2721 (1998).

26. J. Huang, J. Blochwitz-Nimoth, M. Pfeiffer and K. Leo, J. Appl. Phys. **93**, 838 (2003).

27. E. Tutiš, D. Berner, and L. Zuppiroli, J. Appl. Phys. **93**, 4594 (2003).

28. B. Masenelli, E. Tutis, M. N. Bussac, and L. Zuppiroli, Syn. Met. **121**, 1513 (2001).

29. R. Kersting, U. Lemmer, M. Deussen, H. J. Bakker, R. F. Mahrt, H. Kurz, V. I. Arkhipov, H. Bässler, and E. O. Göbel, Phys. Rev. Lett. **73**, 1440 (1994).

30. Y. Luo, H. Aziz, Z. D. Popovic and G. Xu, Appl. Phys. Lett. **89**, 103505 (2006).

31. S. Karg, J. Steiger, and H. von Seggern, Synth. Met. **111-112**, 277 (2000).

32. J. Kakalios, R. A. Street, and W. B. Jackson, Phys. Rev. Lett. **59**, 1037 (1987).

33. D. L. Huber, Phys. Rev. E. **53**, 6544 (1996).

34. H. Park, D. S. Shin, H. S. Yu, and H. B. Chae, Appl. Phys. Lett. **90**, 202103 (2007).

35. C. P. Lindsey and G. D. Patterson, J. Chem. Phys. **73**, 3348 (1980).

36. S. Naka, H. Okada, H. Onnagawa, and T. Tsutsui, Appl. Phys. Lett. **76**, 197 (2000).

37. H. You, Y. Dai, Z. Zhang, and D. Ma, J. Appl. Phys. **101**, 026105 (2007).

38. H. Lee, S. W. Cho, K. Han, P. E. Jeon, C. N. Whang, K. Jeong, K. Cho, and Y. Yi, Appl. Phys. Lett. **93**, 043308 (2008).

39. The spike's peak location can be affected by the time constant or delay time of the electronics. In the low- and room-temperature measurements the coaxial cables connecting the OLED to the electronics are ~4 and ~1.5 m long, so the spikes peak at 200–300 and 100 – 200 ns, respectively.

40. M. A. Baldo and S. R. Forrest, Phys. Rev. B **62**, 10958 (2000).

41. H. Murata, C. D. Merritt and Z. H. Kafafi, IEEE Journal of Selected Topics in Quantum Electronics **4**, 119 (1998).